


Experimental demonstration of optimal unambiguous two-out-of-four quantum state elimination

Jonathan W. Webb, Ittoop V. Puthoor , Joseph Ho, Jonathan Crickmore, Emma Blakely, Alessandro Fedrizzi, and Erika Andersson

Institute of Photonics and Quantum Sciences, School of Engineering and Physical Sciences, Heriot-Watt University, Edinburgh EH14 4AS, United Kingdom



(Received 30 June 2022; revised 10 March 2023; accepted 15 March 2023; published 12 May 2023)

A core principle of quantum theory is that nonorthogonal quantum states cannot be perfectly distinguished with single-shot measurements. However, it is possible to exclude a subset of nonorthogonal states without error in certain circumstances. Here we implement a quantum state elimination measurement which unambiguously rules out two of four pure, nonorthogonal quantum states—ideally without error and with unit success probability. This is a generalized quantum measurement with six outcomes, where each outcome corresponds to excluding a pair of states. Our experimental realization uses single photons, with information encoded in a four-dimensional state using optical path and polarization degrees of freedom. The prepared state is incorrectly ruled out up to 3.3(2)% of the time.

DOI: [10.1103/PhysRevResearch.5.023094](https://doi.org/10.1103/PhysRevResearch.5.023094)

I. INTRODUCTION

Quantum state elimination (QSE) [1–6] aims to exclude one or more quantum states from a given set. Just like for the closely related task of quantum state discrimination [7–13], QSE tasks can be optimized with regard to a number of competing payoffs: For example, minimum-error measurements always return an outcome but sometimes eliminate the wrong state; unambiguous measurements on the other hand never exclude the wrong state, but occasionally return an inconclusive result [1,3,6]. Interestingly, for QSE there exist certain sets of nonorthogonal states where it is possible to both always return an outcome and never exclude the wrong state: This is the regime our work focuses on.

A number of quantum information processing protocols [4,5,14,15] and communication schemes [16,17] have been developed based on QSE. Thus far, QSE-based schemes have been realized using standard projective measurements. For example, one-out-of-two quantum oblivious transfer—where a sender has two bits and a receiver obtains either the first or second bit in such a way that the sender does not know which bit was received—has been demonstrated in Ref. [18]. Additionally, quantum digital signatures provide an information-theoretic secure method of verifying message authenticity amongst users, where projective elimination measurements remove the need for quantum memories [19]. Investigations into the fundamental properties of the wave function also make use of projective exclusion measurements [20]. Namely, the so-called Pusey-Barrett-Rudolph (PBR) theorem introduces a no-go result which shows that quantum

states cannot be regarded as purely statistical descriptions of their underlying physical states.

Eliminating nonorthogonal sets of states is in general more involved and often requires a generalized measurement. An early related result was derived by Caves *et al.* [21], who found the sufficient conditions for when it is possible to unambiguously exclude one of three possible nonorthogonal quantum states with zero failure probability, as well as generalized exclusion of “trine” states—three states that are nonorthogonal and symmetric [2,16,17]. In Ref. [16], elimination measurements on trine states are used in a quantum key distribution protocol.

In this paper, we derive and demonstrate an experimental realization of the optimal quantum state elimination measurement for the four nonorthogonal states considered by Crickmore *et al.* [6]. Furthermore, this is an experimental implementation of a generalization of the PBR measurement [20]. A six-outcome positive operator-valued measurement (POVM) is required where each outcome corresponds to eliminating a unique pair of states. The POVM is mapped onto an optical platform and optimized by minimizing the number of optical elements. Our states are encoded in the path and polarization of single photons. We prepare each of the four possible states, perform the state elimination measurement, and compare the results with theoretical predictions.

II. THEORETICAL FRAMEWORK

Let us consider two qubits, each prepared in one of two states, $|\pm\theta\rangle = \cos\theta|0\rangle \pm \sin\theta|1\rangle$ [6]. The four possible two-qubit states are

$$\begin{aligned} |+\theta, \pm\theta\rangle &= \cos^2\theta|00\rangle \pm \sin^2\theta|11\rangle \\ &\quad \pm \cos\theta\sin\theta(|01\rangle \pm |10\rangle), \\ |-\theta, \pm\theta\rangle &= \cos^2\theta|00\rangle \mp \sin^2\theta|11\rangle \\ &\quad \pm \cos\theta\sin\theta(|01\rangle \mp |10\rangle). \end{aligned} \quad (1)$$

Published by the American Physical Society under the terms of the [Creative Commons Attribution 4.0 International license](https://creativecommons.org/licenses/by/4.0/). Further distribution of this work must maintain attribution to the author(s) and the published article's title, journal citation, and DOI.

This family of two-qubit states represent a generalization of the PBR states [20], which are obtained for $2\theta = 45^\circ$ [6]. When $\cos 2\theta \leq \sqrt{2} - 1$, it is possible to always exclude two of the four states with success probability equal to 1. When $\theta = \cos^{-1}(\sqrt{2} - 1)/2$, the states are the least distinguishable, but still distinguishable enough such that two of them can be perfectly ruled out [6]. This is the case we consider in this paper. For completeness, when $\cos 2\theta > \sqrt{2} - 1$, we can eliminate two of four states with success probability less than 1.

From the set of four states in (1), there are six ways to choose a pair of states, each corresponding to a measurement outcome. Using the shorthand notation “++” for the state $|+\theta, +\theta\rangle$, “+-” for $|+\theta, -\theta\rangle$ and so on, we define the sets

$$\begin{aligned} A &= \{++, +-\}, & B &= \{++, -+\}, \\ C &= \{+-, --\}, & D &= \{-+, --\}, \\ E &= \{+-, -+\}, & F &= \{++, --\}. \end{aligned} \quad (2)$$

The measurement operators are formed from the six nonorthogonal un-normalized states

$$\begin{aligned} |\psi_A\rangle &= \frac{1}{\sqrt{2}}(\sqrt{\sqrt{2}-1}|00\rangle - |10\rangle), \\ |\psi_B\rangle &= \frac{1}{\sqrt{2}}(\sqrt{\sqrt{2}-1}|00\rangle - |01\rangle), \\ |\psi_C\rangle &= \frac{1}{\sqrt{2}}(\sqrt{\sqrt{2}-1}|00\rangle + |01\rangle), \\ |\psi_D\rangle &= \frac{1}{\sqrt{2}}(\sqrt{\sqrt{2}-1}|00\rangle + |10\rangle), \\ |\psi_E\rangle &= \frac{1}{\sqrt{2}}((\sqrt{2}-1)|00\rangle + |11\rangle), \\ |\psi_F\rangle &= \frac{1}{\sqrt{2}}((\sqrt{2}-1)|00\rangle - |11\rangle). \end{aligned} \quad (3)$$

Each of these states are orthogonal to a pair of states in (1). The measurement operators that exclude a pair are given by $\Pi_i = |\psi_i\rangle\langle\psi_i|$, with $i \in \{A, B, C, D, E, F\}$.

This generalized quantum measurement can be realized by extending the four-dimensional Hilbert space to six dimensions and then making a projective measurement in the six-dimensional extended space. The projective measurement in turn can be realized by applying a particular unitary transform U , followed by a projection in the computational basis [22]. For details of this construction, see Appendix A. In short, following Reck *et al.* [23], we decompose the unitary transform as a set of 2×2 beam-splitter-like (BS) operations. This decomposition is optimized by permuting the ordering of the basis states through all possibilities, obtaining the decomposition in each case, and choosing the decomposition with the minimum number of BS operations. We denote these BS operations by matrices T_{ij} with $i, j \in \{1, \dots, 6\}$. The T_{ij} matrices can be physically implemented using beam splitters and wave plates. The decomposition that needs the lowest number of T_{ij} matrices will also result in the minimum number of optical elements in the experiment. The decomposition of the unitary operation is not unique, but other decompositions

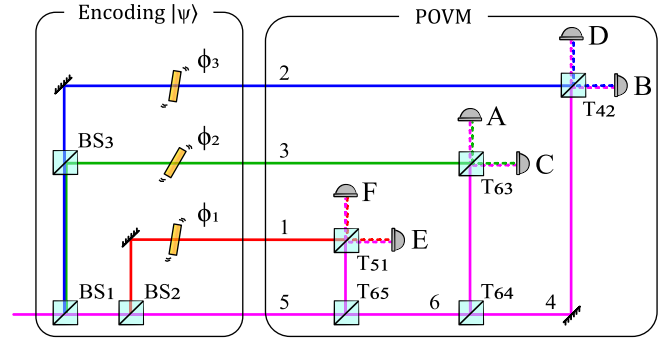


FIG. 1. Two-out-of-four state elimination setup using linear optics. We encode one of the four quantum states in Eq. (1), here denoted $|\psi\rangle$, using BS₁, BS₂, BS₃ and ϕ_1 , ϕ_2 , ϕ_3 , which act on the four path modes corresponding to the basis states $|00\rangle$, $|01\rangle$, $|10\rangle$, $|11\rangle$. The state elimination POVM is realized by acting on the state encoded in the four path modes with the beam splitters T_{ij} as described in the main text. Single-photon detectors monitor the six outcomes A, B, C, D, E, and F.

would lead to a larger number of optical elements. One generally has $UT_{M,M-1}T_{M,M-2}\cdots T_{2,1} = D$, where M is the number of outcomes, here 6, and D is a diagonal matrix.

We will present an optical implementation, as shown in Fig. 1, but the method of constructing the physical realization can be used also for other physical platforms such as atoms or ions [22]. Here, the four basis states are realized using four separable path modes. The four quantum states defined in (1) are encoded using BS_{1,2,3} along with phase shifters ($\phi_{1,2,3}$). After the optical network which realizes the unitary transform U , a click in each of the detectors A–F corresponds to a pair of states being eliminated. The states $|00\rangle$, $|11\rangle$, $|01\rangle$, and $|10\rangle$ are represented by modes 5, 1, 2, and 3, respectively. The auxiliary states, $|\text{aux}_1\rangle$ and $|\text{aux}_2\rangle$, with vacuum states as input, are represented by modes 6 and 4.

III. EXPERIMENT

We encode the quantum states onto single photons produced by a heralded photon-pair source based on parametric downconversion using a periodically poled potassium titanyl phosphate (ppKTP) crystal [24]. Degenerate photon pairs are produced at 1550 nm through using a 775-nm pump from a 80-MHz pulsed Ti-sapphire laser. The two down-converted photons are generated with orthogonal polarization allowing them to be separated by a polarizing beam splitter (PBS) and subsequently coupled into single-mode fiber. As shown in Fig. 2, one of these photons is immediately detected as the herald photon, while the other is sent to the state preparation stage.

We prepare the two-qubit states for the experiment by encoding the four-dimensional Hilbert space onto a single photon, effectively realizing a ququart. The ququart is encoded in the path-mode degree of freedom where colored paths in Fig. 1 directly map to our experimental layout shown in Fig. 2. The four path modes are realized using two calcite beam displacers (BDs), each of which separates an input optical mode into two copropagating paths depending on

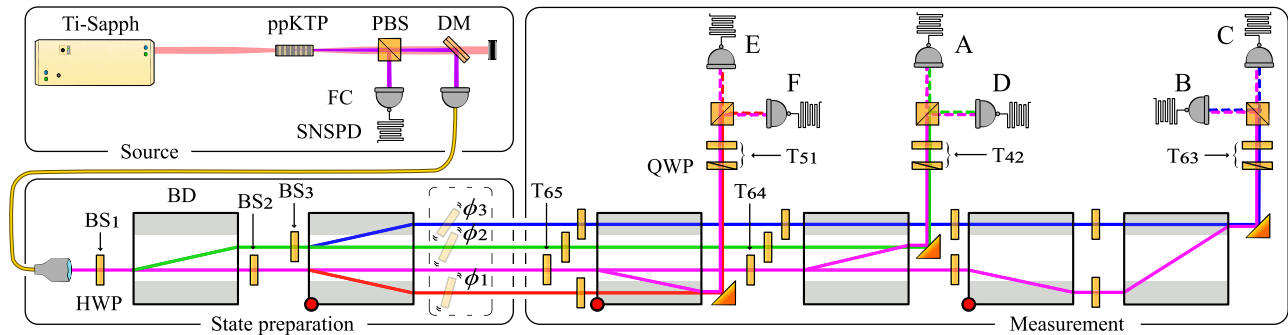


FIG. 2. Experimental layout. A Ti-sapphire (Ti-Sapph) laser pumps a ppKTP crystal to produce a source of single photons. After a dichroic mirror (DM), single photons are coupled to single-mode fiber (FC) and sent to the state preparation stage. Four path modes are formed after two BDs along with HWPs to implement $BS_{1,2,3}$. A BD with a red circle indicates that it is rotated by 90° , while the gray-shaded BD areas denote paths that are vertically offset. The phases $\phi_{1,2,3}$, shown in the dashed box, are deferred to the measurement as described in the main text. The measurement uses HWPs and BDs to implement variable BS operations, $\{T_{65}, T_{64}\}$, on the path modes. Additional HWPs compensate path length differences. The remaining BS operations, $\{T_{51}, T_{42}, T_{63}\}$, are realized in polarization through the use of a quarter-wave plate (QWP), HWP, and PBS. Superconducting nanowire single-photon detectors (SNSPDs) detect the single photons in the six POVM output modes.

their polarization. BD interferometers generally have excellent passive phase stability and are widely used in multipath and polarization encoding in quantum optics setups [25–29]. By using half-wave plates (HWPs) on each path prior to the BD we set the relative splitting ratios of $BS_{1,2,3}$. In the setup, the four paths copropagate in a square lattice, which is achieved by rotating the second BD by 90° with respect to the propagation path, such that the spatial walkoff is in the vertical direction. In the figure, the gray shading indicates the top two path modes, while the unshaded regions represent the bottom two path modes. Ideally, the phase shifts ($\phi_{1,2,3}$) are applied to the path modes directly as shown in Fig. 2 to prepare the different states in (1); see Appendix B for details. The unitary phase shifts ϕ commute with part of the unitary operation forming the POVM. Hence, in the experiment, these phases are implemented in the measurement stage, before the projective measurements and detection.

The POVM involves implementing U on the path modes followed by a projective measurement in the extended basis spanned by the six outcomes. As per the Reck *et al.* [23] decomposition of U , we implement the network of beam splitters, denoted by $T_{i,j}$, using both path and polarization degrees of freedom. We carry out part of the unitary transform on the path modes using BDs and HWPs, similar to the state preparation. Specifically, the BDs spatially combine two path modes of orthogonal polarization, with specific ratios set by the HWPs, into a single path mode. The combined path modes retain orthogonal polarization components, which allows the final part of the unitary to be implemented in polarization. We use right-angle prism mirrors to direct the combined path modes towards polarization measurement stages. These consist of a QWP and HWP which implement the remaining $T_{i,j}$ operations in polarization, as well as $\phi_{1,2,3}$, followed by a PBS for the projective measurement.

Finally, photons in each of the six path modes $A-F$, as defined in (2), are detected with SNSPDs and a counting logic with a 1 ns coincidence window. We conducted measurements with up to 30 s integration time for each experimentally prepared state.

IV. RESULTS

We prepared $\sim 2.3 \times 10^5$ copies for each of the four states defined in (1) and measured the output statistics of the POVM. This is done by recording the number of detection events in each labeled path mode, $A-F$, which corresponds to eliminating a particular pair of states. The experimental outcome probabilities are shown in Fig. 3 and compared with theoretical predictions. For all states, mutually distinguishable sets of three outcomes are expected to have zero probability. This is the signature that allows the unambiguous two-out-of-four state elimination. The probability of the outcomes

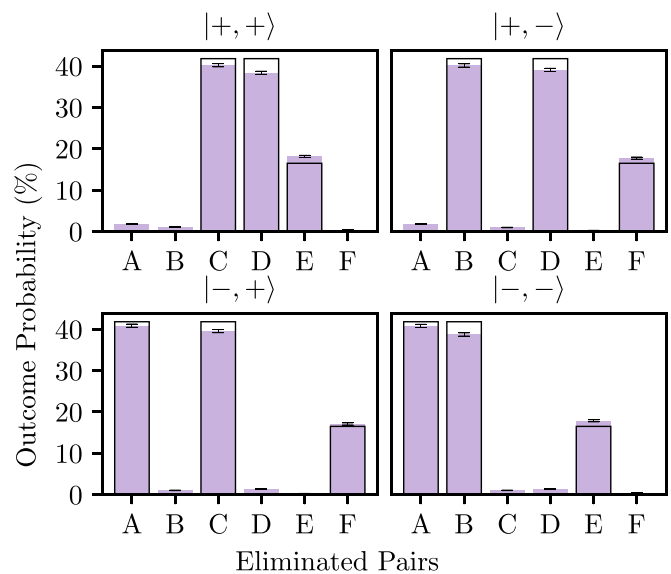


FIG. 3. Experimental results. For each of the states prepared (indicated above each plot) the probability of detecting a photon in the respective output modes $\{A-F\}$ is shown by the filled bars. The theoretically predicted probability is indicated by a black outline. Each letter corresponds to a pair of states being excluded as per (2). Error bars for the experimental data represent three standard deviations assuming Poissonian statistics.

are given by $p_i = \text{Tr}(\Pi_i \rho)$. More details are provided in Appendix A. Ideally, the nonzero outcome probability for each state is $\sqrt{2} - 1 \approx 41.4\%$ for outcomes A – D and $3 - 2\sqrt{2} \approx 17.2\%$ for E and F . This distribution depends on θ , which determines the set of states to be eliminated. If θ is any smaller than the value we have chosen, pairs of states cannot be eliminated without error.

The experimental data demonstrate good agreement with theoretical predictions, with a maximum fractional error rate of 3.3(2)% for the input state, $|++\rangle$, that being the total percentage of erroneous outcomes, which should ideally be 0%. For the remaining states, we observe the total fractional errors of {3.0(2)%, 2.5(2)%, 2.6(2)%} when preparing the states $\{|+-\rangle, |-+\rangle, |--\rangle\}$, respectively. Here, an erroneous outcome for the QSE task is considered to be where the measurement result eliminates a pair of states that includes the input state that is prepared. The main contribution to imperfect elimination probabilities is nonunit visibility in the BD interferometers; on average we observe interference visibilities of 97.7%. This is somewhat lower than can be expected from BD interferometers, owing to the two-dimensional (2D) layout of our optical path modes.

V. DISCUSSION

We have demonstrated the first two-out-of-four state elimination using a generalized quantum measurement and a path-mode encoding scheme for a specific set of states. For both one- and two-out-of-four state elimination, measurements in an entangled basis are known to outperform local measurements (that is, separate measurements on each qubit) [6,20]. Although our measurement would have required entangling operations if realized on two physically separate qubits, here it does not require entangling operations, because we have realized it using a ququart. Although our realization is optical, the same methods can be used to construct realizations of generalized measurements on other platforms, such as trapped ions or atoms [22]. What changes with each physical realization is what the relevant basis states are, and what the physical operations that couple pairs of states are. The matrix decomposition of the unitary U can remain the same, or a different gate decomposition tailored to each experimental context may be used. The principle of extending the system’s Hilbert space, implementing the necessary unitary U , and measuring in the computational basis remains the same for any physical realization. If one wants to maximize the average number of eliminated states from a set of qubits, local measurements are optimal, but in this case, sometimes no states will be eliminated [6]. Unlike previous state elimination measurements, our demonstration realizes a generalized unambiguous measurement.

Quantum state elimination is less explored than state discrimination but has already proven useful as a tool for different quantum information tasks [16,18,19]. Quantum state elimination has applications in quantum cryptography, e.g., in a noninteractive exclusive OR (XOR) oblivious transfer protocol which uses a particular set of qutrit quantum states, selected in order to obtain the smallest possible cheating probabilities for unrestricted dishonest parties [30]. Quantum state elimination among four states may also enable modified

quantum key distribution (QKD) schemes where the secret key bit is created only after the measurement is performed by the receiver—similar to a prior QKD scheme that employs elimination of one among three states [16]. The sender might prepare one of four nonorthogonal states, representing two bit values, and the recipient excludes two of these states, meaning that they learn the first bit, the second bit, or their XOR. Finally, the receiver publicly announces which bit was obtained, but not its value. The two parties then share this secret bit. This QKD scheme is conceptually different from traditional QKD and may be worthy of further study. Theoretically, it has been shown that communication games based on excluding information through state elimination can be “infinitely” more efficient when using a quantum resource rather than a classical resource [14]. For our specific scenario, weak-duality games can be demonstrated where two-out-of-four state elimination is required for a winning strategy [31]. A future direction will be to further explore unambiguous state elimination for different sets of states, as well as for an increasing number of states and dimensions. One approach is to use group theory to study state elimination measurements [32].

ACKNOWLEDGMENTS

We thank Neil Ross for helping design and 3D print components. This work was supported by the EPSRC Quantum Communications Hub (Grant No. EP/T001011/1). J.C. acknowledges support from the EPSRC Condensed Matter Centre for Doctoral Training, Grant No. EP/L015110/1.

APPENDIX A: REALIZING THE POVM

Here we present the details of how we realized the POVM. The mathematical description of the optimal measurement is given by Crickmore *et al.* [6]. When $\cos 2\theta = \sqrt{2} - 1$, meaning that $2\theta \approx 65.5^\circ$, the measurement operators that eliminate each pair of states are given by $\Pi_i = |\psi_i\rangle\langle\psi_i|$, with $i \in \{A, B, C, D, E, F\}$. Here, $|\psi_i\rangle$ are six un-normalized states with $\langle\psi_i|\psi_i\rangle < 1$, which are not orthogonal to each other. Each state $|\psi_i\rangle$ is, however, orthogonal to the pair of states that are excluded when obtaining outcome i . We will realize the pair elimination measurement for this particular value of θ . (When $\cos 2\theta < \sqrt{2} - 1$, some of the measurement operators are mixed.)

Explicitly, we have

$$\begin{aligned}
 |\psi_A\rangle &= \frac{1}{\sqrt{2}}(\sqrt{\sqrt{2}-1}|00\rangle - |10\rangle), \\
 |\psi_B\rangle &= \frac{1}{\sqrt{2}}(\sqrt{\sqrt{2}-1}|00\rangle - |01\rangle), \\
 |\psi_C\rangle &= \frac{1}{\sqrt{2}}(\sqrt{\sqrt{2}-1}|00\rangle + |01\rangle), \\
 |\psi_D\rangle &= \frac{1}{\sqrt{2}}(\sqrt{\sqrt{2}-1}|00\rangle + |10\rangle), \\
 |\psi_E\rangle &= \frac{1}{\sqrt{2}}((\sqrt{2}-1)|00\rangle + |11\rangle), \\
 |\psi_F\rangle &= \frac{1}{\sqrt{2}}((\sqrt{2}-1)|00\rangle - |11\rangle). \tag{A1}
 \end{aligned}$$

1. Completing the matrix

In order to realize this generalized state elimination measurement, we need to translate the above mathematical description of the measurement into a physical setup. The first step is to employ the so-called Neumark extension. In short, this means that a generalized quantum measurement can be realized as a projective measurement in some higher-dimensional Hilbert space; we need as many dimensions as there are outcomes. We first write $|\psi_i\rangle = a_{r,1}|00\rangle + a_{r,2}|01\rangle + a_{r,3}|10\rangle + a_{r,4}|11\rangle$, where $r = 1$ for $i = A$, $r = 2$ for $i = B$, and so on, until $r = 6$ for $i = F$. We then form a 6×4 matrix V with elements $V_{r,j} = a_{r,j}^*$,

$$V = \frac{1}{\sqrt{2}} \begin{pmatrix} \sqrt{\sqrt{2}-1} & 0 & -1 & 0 \\ \sqrt{\sqrt{2}-1} & -1 & 0 & 0 \\ \sqrt{\sqrt{2}-1} & 0 & 1 & 0 \\ \sqrt{\sqrt{2}-1} & 1 & 0 & 0 \\ \sqrt{2}-1 & 0 & 0 & 1 \\ \sqrt{2}-1 & 0 & 0 & -1 \end{pmatrix}. \tag{A2}$$

Why we are doing this will become clear shortly. In the matrix V , the coefficients in each row belong to an un-normalized “measurement state” $|\Psi_i\rangle$, and each column contains the coefficients for one particular basis state.

The completeness condition $\sum_i \Pi_i = 1$ ensures that the probabilities for all results sum to 1, no matter what state is being measured. This condition means that it holds that $\sum_r a_{r,j}^* a_{r,j} = 1$ and $\sum_r a_{r,k}^* a_{r,l} = 0$, where $j, k, l \in \{1, 2, 3, 4\}$ and $k \neq l$. This in turn means that the four columns in the matrix V in Eq. (A2) are four six-dimensional orthonormal vectors. We can then complete the matrix into a 6×6 unitary matrix by adding two more columns, corresponding to six-dimensional vectors which are orthonormal both to each other and to the four existing columns. That is, we add coefficients for two auxiliary basis states, $|\text{aux}_1\rangle$ and $|\text{aux}_2\rangle$. Physically, the auxiliary basis states can be additional degrees of freedom for the existing quantum system(s) or can result from adding one or more auxiliary quantum systems; just a single auxiliary qubit would double the number of basis

states. The mathematical description of how the measurement is realized is the same, but the physical realization is different. In our realization, the four original basis states and the two auxiliary states will all be represented by different spatial modes of a single photon.

If there are two or more columns to add, then this can be done in infinitely many ways. We can, for example, choose

$$U = \begin{pmatrix} | & \frac{1}{2} & \frac{1}{2} - \frac{1}{\sqrt{2}} \\ | & -\frac{1}{2} & \frac{1}{2} - \frac{1}{\sqrt{2}} \\ V & | & \frac{1}{2} & \frac{1}{2} - \frac{1}{\sqrt{2}} \\ | & -\frac{1}{2} & \frac{1}{2} - \frac{1}{\sqrt{2}} \\ | & 0 & \sqrt{\sqrt{2}-1} \\ | & 0 & \sqrt{\sqrt{2}-1} \end{pmatrix}. \tag{A3}$$

No matter exactly how we choose to complete the unitary matrix V , to give a particular U , it then holds that

$$\langle i|U\rho U^\dagger|i\rangle = \langle \psi_i|\rho|\psi_i\rangle = \text{Tr}(\Pi_i\rho) = p_i, \tag{A4}$$

where $|i\rangle$ is the basis vector corresponding to the i th basis state and ρ is a state with support only in the four-dimensional “original” Hilbert space. This means that the measurement can be physically realized by performing U on the original system, coupling it to the auxiliary degrees of freedom, followed by making a projective measurement in the basis given by the four original basis states plus the two auxiliary ones.

2. Decomposing the unitary operation into optical elements

We search for a decomposition of U containing the smallest possible number of T matrices. By permuting input and output basis states before decomposing U using the method in Ref. [23], decompositions with different numbers of T matrices can be obtained. We look for a realization with as few optical elements as possible. We denote the matrix obtained from U by permuting input and output basis states, giving the smallest number of optical elements, by U_{opt} . The decomposition is then determined by $D = U_{\text{opt}}T_{65}T_{64}T_{63}T_{51}T_{42}$, where D is a diagonal matrix and the remaining T matrices are identity operations. We have

$$U_{\text{opt}} = \begin{pmatrix} -\frac{1}{\sqrt{2}} & 0 & 0 & 0 & \sqrt{\sqrt{2}-1} & 1 - \frac{1}{\sqrt{2}} \\ 0 & -\frac{1}{\sqrt{2}} & 0 & -\frac{1}{2} & \frac{1}{2} - \frac{1}{\sqrt{2}} & \sqrt{\frac{1}{\sqrt{2}} - \frac{1}{2}} \\ 0 & 0 & -\frac{1}{\sqrt{2}} & \frac{1}{2} & \frac{1}{2} - \frac{1}{\sqrt{2}} & \sqrt{\frac{1}{\sqrt{2}} - \frac{1}{2}} \\ 0 & \frac{1}{\sqrt{2}} & 0 & -\frac{1}{2} & \frac{1}{2} - \frac{1}{\sqrt{2}} & \sqrt{\frac{1}{\sqrt{2}} - \frac{1}{2}} \\ \frac{1}{\sqrt{2}} & 0 & 0 & 0 & \sqrt{\sqrt{2}-1} & 1 - \frac{1}{\sqrt{2}} \\ 0 & 0 & \frac{1}{\sqrt{2}} & \frac{1}{2} & \frac{1}{2} - \frac{1}{\sqrt{2}} & \sqrt{\frac{1}{\sqrt{2}} - \frac{1}{2}} \end{pmatrix}. \tag{A5}$$

The T matrices are given by

$$\begin{aligned}
 T_{65} &= \begin{pmatrix} 1 & 0 & 0 & 0 & 0 & 0 \\ 0 & 1 & 0 & 0 & 0 & 0 \\ 0 & 0 & 1 & 0 & 0 & 0 \\ 0 & 0 & 0 & 1 & 0 & 0 \\ 0 & 0 & 0 & 0 & 0.91 & -0.414 \\ 0 & 0 & 0 & 0 & 0.414 & 0.91 \end{pmatrix}, & T_{63} &= \begin{pmatrix} 1 & 0 & 0 & 0 & 0 & 0 \\ 0 & 1 & 0 & 0 & 0 & 0 \\ 0 & 0 & \frac{1}{\sqrt{2}} & 0 & 0 & \frac{1}{\sqrt{2}} \\ 0 & 0 & 0 & 1 & 0 & 0 \\ 0 & 0 & 0 & 0 & 1 & 0 \\ 0 & 0 & -\frac{1}{\sqrt{2}} & 0 & 0 & \frac{1}{\sqrt{2}} \end{pmatrix}, & T_{42} &= \begin{pmatrix} 1 & 0 & 0 & 0 & 0 & 0 \\ 0 & \frac{1}{\sqrt{2}} & 0 & \frac{1}{\sqrt{2}} & 0 & 0 \\ 0 & 0 & 1 & 0 & 0 & 0 \\ 0 & -\frac{1}{\sqrt{2}} & 0 & \frac{1}{\sqrt{2}} & 0 & 0 \\ 0 & 0 & 0 & 0 & 1 & 0 \\ 0 & 0 & 0 & 0 & 0 & 1 \end{pmatrix}, \\
 T_{64} &= \begin{pmatrix} 1 & 0 & 0 & 0 & 0 & 0 \\ 0 & 1 & 0 & 0 & 0 & 0 \\ 0 & 0 & 1 & 0 & 0 & 0 \\ 0 & 0 & 0 & \frac{1}{\sqrt{2}} & 0 & \frac{1}{\sqrt{2}} \\ 0 & 0 & 0 & 0 & 1 & 0 \\ 0 & 0 & 0 & -\frac{1}{\sqrt{2}} & 0 & \frac{1}{\sqrt{2}} \end{pmatrix}, & T_{51} &= \begin{pmatrix} -\frac{1}{\sqrt{2}} & 0 & 0 & 0 & \frac{1}{\sqrt{2}} & 0 \\ 0 & 1 & 0 & 0 & 0 & 0 \\ 0 & 0 & 1 & 0 & 0 & 0 \\ 0 & 0 & 0 & 1 & 0 & 0 \\ -\frac{1}{\sqrt{2}} & 0 & 0 & 0 & -\frac{1}{\sqrt{2}} & 0 \\ 0 & 0 & 0 & 0 & 0 & 1 \end{pmatrix}. & & & & & & (A6)
 \end{aligned}$$

APPENDIX B: EXPERIMENTAL DETAILS

Details of how the experiment was performed are presented, starting from how we prepared the initial state.

1. State preparation

The states to be prepared were given in (1); that is, they are

$$\begin{aligned}
 |+\theta, \pm\theta\rangle &= \cos^2\theta|00\rangle \pm \sin^2\theta|11\rangle \\
 &\quad \pm \cos\theta \sin\theta(|01\rangle \pm |10\rangle), \\
 |-\theta, \pm\theta\rangle &= \cos^2\theta|00\rangle \mp \sin^2\theta|11\rangle \\
 &\quad \pm \cos\theta \sin\theta(|01\rangle \mp |10\rangle). & (B1)
 \end{aligned}$$

To see how these states are prepared in our implementation, consider Fig. 1, where each basis state $|00\rangle, |01\rangle, |10\rangle, |11\rangle$ represents one of the four colored path modes. The blue line represents the state $|01\rangle$, green represents $|10\rangle$, red represents $|11\rangle$, and purple represents $|00\rangle$. Phase shifts of ± 1 only need to be applied to the basis states $|11\rangle, |10\rangle$, and $|01\rangle$. The phase shifts are achieved by adding a phase change to the appropriate path in an interferometer in our setup. As the basis state $|00\rangle$ requires no sign change, no phase shift is needed on the purple mode.

Preparing one of the four states in (1) is achieved by rotating a HWP, corresponding to a phase shift, by π , or not rotating it. The notation $\phi_i, i = \{1, 2, 3\}$, is the same as in Fig. 1. Each state is prepared through applying a rotation in a certain combination outlined in Table I. As an example,

TABLE I. Preparation of a state through applying a phase to an arm of each MZI.

Desired state	ϕ_1	ϕ_2	ϕ_3
$ +\theta, +\theta\rangle$	0	0	0
$ +\theta, -\theta\rangle$	π	0	π
$ -\theta, +\theta\rangle$	π	π	0
$ -\theta, -\theta\rangle$	0	π	π

if preparing $|+\theta, +\theta\rangle$, the phase shifts are all $+1$; that is, no phase shift is required. Hence $\phi_i, i = \{1, 2, 3\}$, impart no rotation.

Experimentally, we implement this operation by pushing the phase shift from a separable operation as seen in Fig. 1 in the main text to one combined with the T_{51}, T_{42} , and T_{63} operations. This is done out of experimental convenience and is true to Fig. 1 in the main text. To see this, one could realize the same experimental setup but separate the T operations from the phase shift operations by introducing a QWP-HWP-QWP configuration, giving access to the entire Poincaré sphere, prior to the HWP that makes up the projection along with the PBS, which would allow for explicit realization of the phase shift operation. The two path modes' polarization is still individually accessible as they have yet to combine on the final HWP. Hence the operation of the QWP and HWP prior to the PBS is sufficient to perform the T operations along with the phase shift operations.

In order for the states to be prepared correctly and for the probability amplitudes of a photon detection at each detector to be balanced, BS operations are performed at the encoding stage. To be explicit, consider the following example with reference to Fig. 1 in the main text. The Mach-Zehnder interferometer (MZI) made up of the red- and purple-colored path modes needs to be balanced in terms of probability. That is, the red path is made a transmission through BS_1 and reflection through BS_2 , and the purple path is composed of transmission through BS_1 and BS_2 and reflection of T_{65} . The BS and

TABLE II. The theoretical ratios between transmission and reflection each variable BS operates on their respective path modes.

BS operation	Transmission (%)	Reflection (%)
BS_1	58.58	42.42
BS_2	85.36	14.64
BS_3	50.00	50.00
T_{65}	82.81	16.81
T_{64}	50.00	50.00

TABLE III. Probability amplitude distribution along each arm. The detector set consisting of E and F has a total probability of 16.99% of the total incident probability amplitude. The detector set consisting of A and C and the detector set consisting of B and D take 41.91% of the total incident probability amplitude. We see a total percentage higher than 100%. These values are derived from Table II and are susceptible to rounding errors. Experimentally, we are trying to balance each arm in accordance with these values, and so this table is used more as a guide than as a definite limit.

Detector set	Path color	Probability amplitude (%)
E and F	Red	8.58
	Purple	8.41
A and C	Green	21.21
	Purple	20.7
D and B	Blue	21.21
	Purple	20.7
Total		100.81

T_{65} operations should have beam splitter ratios that direct some amount of probability to not only balance the arms, but also give up enough probability amplitude to the other two interferometers. Our method of determining how to balance each interferometer, i.e., how to determine the transmission and reflection coefficients of each beam splitting operation, is found via mode expansion. The T matrix operations were presented previously along with the BS operations BS_i , where $i = \{1, 2, 3\}$, below, which allow us to model a condition where each interferometer is balanced.

$$\begin{aligned}
 BS_1 &= \begin{pmatrix} \sqrt{\cos^4 \theta + \sin^4 \theta} & -\sqrt{2} \cos \theta \sin \theta \\ \sqrt{2} \cos \theta \sin \theta & \sqrt{\cos^4 \theta + \sin^4 \theta} \end{pmatrix}, \\
 BS_2 &= \frac{1}{\sqrt{\cos^4 \theta + \sin^4 \theta}} \begin{pmatrix} \cos^2 \theta & -\sin^2 \theta \\ \sin^2 \theta & \cos^2 \theta \end{pmatrix}, \\
 BS_3 &= \frac{1}{\sqrt{2}} \begin{pmatrix} 1 & -1 \\ 1 & 1 \end{pmatrix}. \tag{B2}
 \end{aligned}$$

The theoretical values for the transmission and reflection coefficients are given in Table II. This table gives the coefficients for the T matrix operations that take from the purple path mode in Fig. 1 in the main text. The transmission and reflection values can be adjusted depending on setup-specific losses. These values are a starting point and do not take into

TABLE IV. For each prepared state, the probability amplitudes recovered from the single-photon detections are presented along with their uncertainty. This experimental measurement uncertainty for detectors $A-F$ is given by three standard deviations of the detector sets' probability amplitudes assuming Poissonian statistics. The total probability of getting a wrong result is defined as the sum over the probability amplitudes of the detectors that are not meant to click for a given state.

State	Probability outcome of each detector (%)						Total probability error (%)
	A	B	C	D	E	F	
$ +\theta, +\theta\rangle$	1.82(8)	1.09(6)	40.2(4)	38.4(4)	18.2(3)	0.35(4)	3.3(2)
$ +\theta, -\theta\rangle$	0.95(6)	40.2(4)	0.95(6)	39.1(4)	0.24(3)	17.7(3)	3.0(2)
$ -\theta, +\theta\rangle$	40.9(4)	1.00(6)	39.5(4)	1.29(7)	0.24(3)	17.1(3)	2.5(2)
$ -\theta, -\theta\rangle$	40.8(4)	38.7(4)	1.01(6)	1.27(7)	17.8(3)	0.36(4)	2.6(2)

TABLE V. The contrast values for each port leading to a detector. These were found as follows: By coupling a 1550-nm diode laser into each of the ports and by projecting H and V polarizations through the PBS using a HWP, we can obtain the maximum and minimum values for each transmission and reflection port. By using $(I_{\max} - I_{\min}) / (I_{\max} + I_{\min})$, where I is the intensity, we obtain the contrast.

Detector	Contrast (%)
A	98.4
B	96.4
C	98.2
D	97.0
E	97.2
F	98.8

account experimental losses; however, they can be further optimized dependent on the experimental setup.

Using this table, we can examine the percentage of the total probability amplitude available dedicated to each MZI. To be explicit, by following the path using Fig. 1 in the main text as a map, the total probability amplitude the arms of each MZI have is found by multiplying the probabilities in Table II. For example, the first MZI whose output ports are measured by detectors E and F are made up of the red and purple paths. To reiterate, the red path is made from a transmission of BS_1 , which has a transmission probability of 58.58%, and a reflection of BS_2 , which has a reflection probability of 14.64%. This makes the red path have a probability amplitude of 8.58% of the total incident amplitude. Each path with its associated probability amplitude of the total incident amplitude is presented in Table III.

It can be seen in Fig. 1 that the red path mode, making up the interferometer with outcomes E and F , is formed purely off the common purple path. This is the physical cause of why the outcome probability amplitudes are unequal across the nonzero outcomes. Table IV presents our outcomes when each state is prepared, specifically the data that are represented in Fig. 3 in the main text.

2. Additional experimental details

All path modes copropagate in parallel through the BDs, minimizing any mismatch in optical path length and providing passive phase stability on all path modes. In order to operate on the correct path mode in a setup whose compact-

ness is defined by the size of the BD diameter, holed HWPs are used with custom 3D-printed mounts. These plastic 3D prints are subject to large thermal fluctuations and cause drift in the interferometer, reducing the visibility of each interferometer over time. We regard this as the more dominant source of error, which could be mitigated by improving the mounting material from plastic to a higher-thermal-resistance material. We remark that the BD path-mode separation and recombination are determined by the orthogonal polarization components. Importantly, this means that the two optical modes, which are spatially overlapped after the BD, remain distinguishable in the polarization degree of freedom. This is also what forms our six-dimensional Hilbert space through using four spatial modes and two polarization modes. For each outcome, being consistent with the coloring in the previ-

ous figures, we have detector pair $\{E, F\}$: purple-H, red-V, pair $\{A, C\}$: purple-V, green-H, and pair $\{D, B\}$: purple-V, blue-H, where H and V refer to horizontal and vertical polarizations.

Each MZI has associated noise, which can be defined by the contrast, which is dependent on the PBS that closes the MZI. This is also due to an accumulative buildup on nonperfect fringe visibilities of the BDs. Table V shows the contrast of each port associated with a detector.

It should also be noted that manufacturing constraints of the BDs add to the technical limitations of our setup. Ideally, BDs should be matched such that they are mined from the same vein. Imperfect alignment in the lattice structure leads to dephasing which will limit the contrast of the interferometer.

-
- [1] S. Bandyopadhyay, R. Jain, J. Oppenheim, and C. Perry, Conclusive exclusion of quantum states, *Phys. Rev. A* **89**, 022336 (2014).
- [2] S. Barnett, *Quantum Information* (Oxford University Press, Oxford, 2009), pp. 103–104.
- [3] P. Wallden, V. Dunjko, and E. Andersson, Minimum-cost quantum measurements for quantum information, *J. Phys. A: Math. Theor.* **47**, 125303 (2014).
- [4] T. Heinosaari and O. Kerppo, Antidistinguishability of pure quantum states, *J. Phys. A: Math. Theor.* **51**, 365303 (2018).
- [5] V. Havlíček and J. Barrett, Simple communication complexity separation from quantum state antidistinguishability, *Phys. Rev. Res.* **2**, 013326 (2020).
- [6] J. Crickmore, I. V. Puthoor, B. Ricketti, S. Croke, M. Hillery, and E. Andersson, Unambiguous quantum state elimination for qubit sequences, *Phys. Rev. Res.* **2**, 013256 (2020).
- [7] C. W. Helstrom, Quantum detection and estimation theory, *J. Stat. Phys.* **1**, 231 (1969).
- [8] I. D. Ivanovic, How to differentiate between non-orthogonal states, *Phys. Lett. A* **123**, 257 (1987).
- [9] A. Peres, How to differentiate between non-orthogonal states, *Phys. Lett. A* **128**, 19 (1988).
- [10] D. Dieks, Overlap and distinguishability of quantum states, *Phys. Lett. A* **126**, 303 (1988).
- [11] A. Peres and D. R. Terno, Optimal distinction between non-orthogonal quantum states, *J. Phys. A: Math. Gen.* **31**, 7105 (1998).
- [12] S. M. Barnett and S. Croke, Quantum state discrimination, *Adv. Opt. Photon.* **1**, 238 (2009).
- [13] J. A. Bergou, U. Herzog, and M. Hillery, Discrimination of quantum states, in *Quantum State Estimation* (Springer, New York, 2004), Chap. 11, pp. 417–465.
- [14] C. Perry, R. Jain, and J. Oppenheim, Communication Tasks with Infinite Quantum-Classical Separation, *Phys. Rev. Lett.* **115**, 030504 (2015).
- [15] T. Heinosaari and O. Kerppo, Communication of partial ignorance with qubits, *J. Phys. A: Math. Theor.* **52**, 395301 (2019).
- [16] S. J. Phoenix, S. M. Barnett, and A. Chefles, Three-state quantum cryptography, *J. Mod. Opt.* **47**, 507 (2000).
- [17] K. Flatt, S. Croke, and S. M. Barnett, Two-time state formalism for quantum eavesdropping, *Phys. Rev. A* **98**, 052339 (2018).
- [18] R. Amiri, R. Stárek, D. Reichmuth, I. V. Puthoor, M. Mičuda, L. Mišta Jr, M. Dušek, P. Wallden, and E. Andersson, Imperfect 1-out-of-2 quantum oblivious transfer: Bounds, a protocol, and its experimental implementation, *PRX Quantum* **2**, 010335 (2021).
- [19] R. J. Collins, R. J. Donaldson, V. Dunjko, P. Wallden, P. J. Clarke, E. Andersson, J. Jeffers, and G. S. Buller, Realization of Quantum Digital Signatures without the Requirement of Quantum Memory, *Phys. Rev. Lett.* **113**, 040502 (2014).
- [20] M. F. Pusey, J. Barrett, and T. Rudolph, On the reality of the quantum state, *Nat. Phys.* **8**, 475 (2012).
- [21] C. M. Caves, C. A. Fuchs, and R. Schack, Conditions for compatibility of quantum-state assignments, *Phys. Rev. A* **66**, 062111 (2002).
- [22] S. Franke-Arnold, E. Andersson, S. M. Barnett, and S. Stenholm, Generalized measurements of atomic qubits, *Phys. Rev. A* **63**, 052301 (2001).
- [23] M. Reck, A. Zeilinger, H. J. Bernstein, and P. Bertani, Experimental Realization of Any Discrete Unitary Operator, *Phys. Rev. Lett.* **73**, 58 (1994).
- [24] F. Graffitti, P. Barrow, M. Proietti, D. Kundys, and A. Fedrizzi, Independent high-purity photons created in domain-engineered crystals, *Optica* **5**, 514 (2018).
- [25] L. Xiao, X. Qiu, K. Wang, Z. Bian, X. Zhan, H. Obuse, B. C. Sanders, W. Yi, and P. Xue, Higher winding number in a nonunitary photonic quantum walk, *Phys. Rev. A* **98**, 063847 (2018).
- [26] L. Xiao, T. Deng, K. Wang, G. Zhu, Z. Wang, W. Yi, and P. Xue, Non-Hermitian bulk–boundary correspondence in quantum dynamics, *Nat. Phys.* **16**, 761 (2020).
- [27] H. Gao, H. Xue, Q. Wang, Z. Gu, T. Liu, J. Zhu, and B. Zhang, Observation of topological edge states induced solely by non-Hermiticity in an acoustic crystal, *Phys. Rev. B* **101**, 180303(R) (2020).
- [28] M. Ringbauer, T. R. Bromley, M. Cianciaruso, L. Lami, W. Y. S. Lau, G. Adesso, A. G. White, A. Fedrizzi, and M. Piani, Certification and Quantification of Multilevel Quantum Coherence, *Phys. Rev. X* **8**, 041007 (2018).
- [29] M. Ringbauer, B. Duffus, C. Branciard, E. G. Cavalcanti, A. G. White, and A. Fedrizzi, Measurements on the reality of the wavefunction, *Nat. Phys.* **11**, 249 (2015).

- [30] L. Stroh, N. Horová, R. Stárek, I. V. Puthoor, M. Mičuda, M. Dušek, and E. Andersson, Non-interactive XOR quantum oblivious transfer: Optimal protocols and their experimental implementations, [arXiv:2209.11300](https://arxiv.org/abs/2209.11300) [PRX Quantum (to be published)].
- [31] M. Hillery, Partial particle and wave information and weak duality games, *J. Phys. A: Math. Theor.* **54**, 495301 (2021).
- [32] M. Hillery, E. Andersson, and I. Vergheese, A group-theoretic approach to elimination measurements of qubit sequences, [arXiv:2002.02055](https://arxiv.org/abs/2002.02055).